



Facile synthesis of cerium doped Co-Mn-FeO nano ferrites as highly sensitive and fast response humidity sensors at room temperature

S.A. Al-Ghamdi

Advanced Materials Research Laboratory, Department of Physics, Faculty of Science, University of Tabuk, Tabuk 71491, Saudi Arabia

ARTICLE INFO

Keywords:

Rare earth (RE)
Cerium nanoparticles
Solution combustion method
Sensitivity
Humidity sensors

ABSTRACT

Herein, this work presents the facile synthesis of Cerium (Ce^{3+}) doped Cobalt-manganese-iron oxide ferrite as an effective humidity sensor operated at ambient temperature. This work reports, one step solution combustion technique to synthesize $\text{Co}_{0.5}\text{Mn}_{0.5}\text{Fe}_{2-x}\text{Ce}_x\text{O}_4$ ($x = 0.0, 0.050$ and 0.1) ferrites. The structural and morphological features of the synthesized $\text{Co}_{0.5}\text{Mn}_{0.5}\text{Fe}_{2-x}\text{Ce}_x\text{O}_4$ ferrites NPs were investigated through scanning electron microscope (SEM), X-ray diffraction (XRD), Fourier transform infrared spectroscopy (FTIR) and ultraviolet visible (UV-visible) spectroscopy. The XRD results indicates the creation of single phase in pure $\text{Co}_{0.5}\text{Mn}_{0.5}\text{Fe}_{2-x}\text{Ce}_x\text{O}_4$ ferrite that remains unchanged by the mechanism of Ce^{3+} inclusion. The humidity sensing mechanism was systematically investigated using adsorption-desorption isotherms. Highest humidity sensing response was achieved for $\text{Co}_{0.5}\text{Mn}_{0.5}\text{Fe}_{2-x}\text{Ce}_x\text{O}_4$ ($x = 0.1$) ferrite of the order of 98 % in comparison to the pure $\text{Co}_{0.5}\text{Mn}_{0.5}\text{Fe}_{2-x}\text{Ce}_x\text{O}_4$ ($x = 0$) which is about 41 %. The sensors response and recovery times for the $\text{Co}_{0.5}\text{Mn}_{0.5}\text{Fe}_{2-x}\text{Ce}_x\text{O}_4$ ($x = 0.1$) was recorded to be 36 s and 63 s respectively and the sensors long term stability was examined for a duration of 90 days. The results of the present investigation offer new dimensions to fabricate high performance, room temperature operable humidity sensors for next generation sensors applications.

1. Introduction

Water is a universal major element found on the earth surface. Depends on it, for different persistence of both natural and man-made things finds important applications (Kanna et al., 2019). Determination of relative humidity in water content in different materials related to variable environmental conditions are the prime requirement for diverse technological applications (Sakthipandi et al., 2022). The relative humidity measurement plays a prominent role in various fields like environmental monitoring, agricultural activities, food processing, breath monitoring, baby diaper wetting detection and in soil moisture tests etc (Ahilandeswari et al., 2023). The presence of moisture in the surrounding environment can produce oxidation mechanism, which effects the modifications in characteristics properties of the materials. Hence, a quick responding and more sensitivity humidity sensor is required for rapid detection towards regulating the advanced applications (Rezlescu et al., 2005). Generally, humidity sensors can be divided in to five categories like hygrometric, resistive, capacitive, gravimetric, and optical sensors respectively (Blank et al., 2016). The resistive type of humidity sensors is do have number of advantages like economical, quick response, easy method of synthesis, easy to fabricate, and tuneable

electric and magnetic properties (Pratibha et al., 2020a,b). Therefore, they have received important application such as humidity sensors. A number of reports in literature utilized transition metal oxide resistive humidity sensors like titanium oxide (TiO_2), tungsten oxide (WO_3), zinc oxide (ZnO), and iron oxide (Fe_2O_3). This kind of material gives a stable detection range in the order of relative humidity (RH) 20–80 % (Manjunatha et al., 2019a,b). Nanomaterials as humidity sensors have gained advanced and growth based on materials like transition metal oxides (TMOs), graphene and conducting polymers etc (Lakshmiarasanna et al., 2020). The transition metal oxides (TMOs) based nanocomposites have grabbed more attention of scientists and technocrats throughout the globe for the utilization of active material for sensors applications due to their extraordinary morphological properties, improved sensitivity, eco-friendly nature, and easy synthesis (Angadi et al., 2021). Among various TMOs, cobalt-manganese-iron oxide is considered a more appropriate materials for humidity sensors with practical applications because of their more oxidations states in cobalt oxide ($\text{Co}^{3+}/\text{Co}^{2+}$), superior water absorption capacity, tuneable electrical and magnetic features, and improved of thermal stability against to the harsh environment (Sathisha et al., 2020). At present-day, it is huge task to synthesis a new nano features-based ferrites composite

E-mail address: saalghamdi@ut.edu.sa.

<https://doi.org/10.1016/j.jksus.2024.103537>

Received 15 March 2024; Received in revised form 20 June 2024; Accepted 11 November 2024

Available online 14 November 2024

1018-3647/© 2024 The Author(s). Published by Elsevier B.V. on behalf of King Saud University. This is an open access article under the CC BY-NC-ND license (<http://creativecommons.org/licenses/by-nc-nd/4.0/>).

material in the sensor's device fabrication (Manjunatha et al., 2020).

The perovskite kind of ferrite nanocomposites are very prominent in humidity sensing applications due to their morphological features, electrical and optical features. The geometry processed by these ferrites are suitable for many of the technological applications such as gas sensors, solar cells, opto-electronics, and in energy storage devices like supercapacitors (Jagadeesha Angadi et al., 2016). The perovskite geometry is usually represented by ABO_3 , with A and B represents the rare earth (RE) sites like samarium, lanthanum, caesium, yttrium and etc and neodymium transition metals like iron, cobalt, nickel, and manganese (Jagadeesha Angadi et al., 2020). The presence of large number of vacancies in the crystal structure of oxygen lattice plays a major contribution in the electric charge storage kinematics (Ali et al., 2014). At present, the materials based on rare-earth metal oxide have been gaining significant interest due to their water vapour absorption at the active sites (Lodhi et al., 2014).

Recently, K. Manjunatha et al. synthesized $NiFe_2O_4/CoCr_2O_4$ nanocomposites with different concentrations of cobalt and nickel NPs through solution combustion technique. They reported that doping of NPs into ferrite structure significantly improved the humidity sensing performance, with sensitivity 89 % and a response time of 10 s (Manjunatha et al., 2024). Veeresh G. Hiremath, et al. synthesized and fabricated humidity sensors based on $Mg_xRb_{1-x}Fe_2O_4$ ($x = 0.025$ to 0.1) (Hiremath et al., 2022). They reported a highest sensitivity of 93 % for $x = 0.1$ sample with a response time of 15 s. V. Manikandan et al. prepared tin doped nickel-iron ferrite films by using chemical spray pyrolysis method for high performance humidity sensor application (Manikandan et al., 2018). The prepared tin doped nickel-iron ferrite films shows highest sensitivity of 89 % with improved humidity sensing response.

The previous works on humidity sensors based on ferrites discussed above motivated to fabricate a high-performance, rapid detecting humidity sensor based on ferrites such cobalt-manganese-iron-oxide doped with Cerium. In this work, it is proposed to enhance the humidity sensors performance of $Co_{0.5}Mn_{0.5}Fe_{2-x}Ce_xO_4$ ferrites by doping of cerium NPs.

This work report for first time the synthesis of novel cerium (Ce^{3+}) doped $Co_{0.5}Mn_{0.5}Fe_{2-x}Ce_xO_4$ ferrite via solution combustion method for humidity sensing applications. This study reports the detailed investigations into surface morphology, structural features, and sensing behaviour of the cerium doped $Co_{0.5}Mn_{0.5}Fe_{2-x}Ce_xO_4$ ferrite. The cerium (Ce^{3+}) NPs doping in to the $Co_{0.5}Mn_{0.5}Fe_{2-x}Ce_xO_4$ ferrite, results in significant improvement in the humidity sensors features of $Co_{0.5}Mn_{0.5}Fe_{2-x}Ce_xO_4$ ferrite. Among different samples prepared, $Co_{0.5}Mn_{0.5}Fe_{2-x}Ce_xO_4$ ($x = 0.1$) shows 98 % of sensitivity and stable sensing response for 90 days of operation. By measuring the parameters like humidity hysteresis, long term stability tests and response and recovery times, the sensing performance was evaluated using appropriate mathematical equations (Chethan et al., 2019).

As there was no literature on $Co_{0.5}Mn_{0.5}Fe_{2-x}Ce_xO_4$ ferrites-based materials for humidity sensing applications, this is first ever effort to synthesize $Co_{0.5}Mn_{0.5}Fe_{2-x}Ce_xO_4$ ($x = 0.0, 0.050$ and 0.1) ferrite that demonstrates the rapid humidity detection at room temperature.

2. Experimental

2.1. Materials and methods

The raw chemicals such as cobalt nitrate hexahydrate [$Co(NO_3)_2 \cdot 6H_2O$], manganese-based nitrate dihydrate [$Mn(NO_3)_2 \cdot 9H_2O$], ferrous based nitrate nano hydrate [$Fe(NO_3)_3 \cdot 9H_2O$], cerium nitrate [$Ce(NO_3)_3$], glucose [$C_6H_{12}O_6$] and urea [$CO(NH_2)_2$] were purchased from Sigma Aldrich chemical company (South India).

2.2. Synthesis of cerium (Ce^{3+}) doped cobalt-manganese-iron ferrites

In this work, the solution combustion technique was used to

synthesis $Co_{0.5}Mn_{0.5}Fe_{2-x}Ce_xO_4$ ($x = 0.0, 0.050$ and 0.1) ferrite-based NPs. Throughout the synthesis process we have maintained 1:1 M ratio of ferrites and fuels respectively to obtain highly pure $Co_{0.5}Mn_{0.5}Fe_{2-x}Ce_xO_4$ nanoparticles powder.

During synthesis, the urea and glucose acts as reducing agents whereas oxidizing agent is metal nitrate salt. The two oxidizing and reducing agents were taken in appropriate stoichiometric ratios in 500 mL round shaped conical flask. The mixture was stirred for 2 h on a magnetic stirrer at 2000 rpm to attain homogeneous dispersion. The resulting solution of ferrite was shifted to a muffle furnace and heated at a temperature of $500^\circ C$ for 2 h. This nano ferrite solution allowed to boil at high temperature to remove the poisonous gases, the resulting dried mass is used as final product (Chethan et al., 2019). The detailed mechanism of synthesis techniques of $Co_{0.5}Mn_{0.5}Fe_{2-x}Ce_xO_4$ ferrite is shown in the Fig. 1. The final product of nano ferrite was then transferred to a agate mortar and well grinded to obtain a fine ferrite nano powder. This Ce^{3+} doped cobalt-manganese-iron oxide samples were used to perform structural, morphological, and humidity sensing studies. To measure humidity sensing parameters, doped ferrite pellets of dimension $8\text{ mm} \times 1.5\text{ mm}$ were used to test the humidity sensors applications.

2.3. Materials characterization

The surface morphology of $Co_{0.5}Mn_{0.5}Fe_{2-x}Ce_xO_4$ ($x = 0.0, 0.050$ and 0.1) ferrite was analysed by using scanning electron microscope

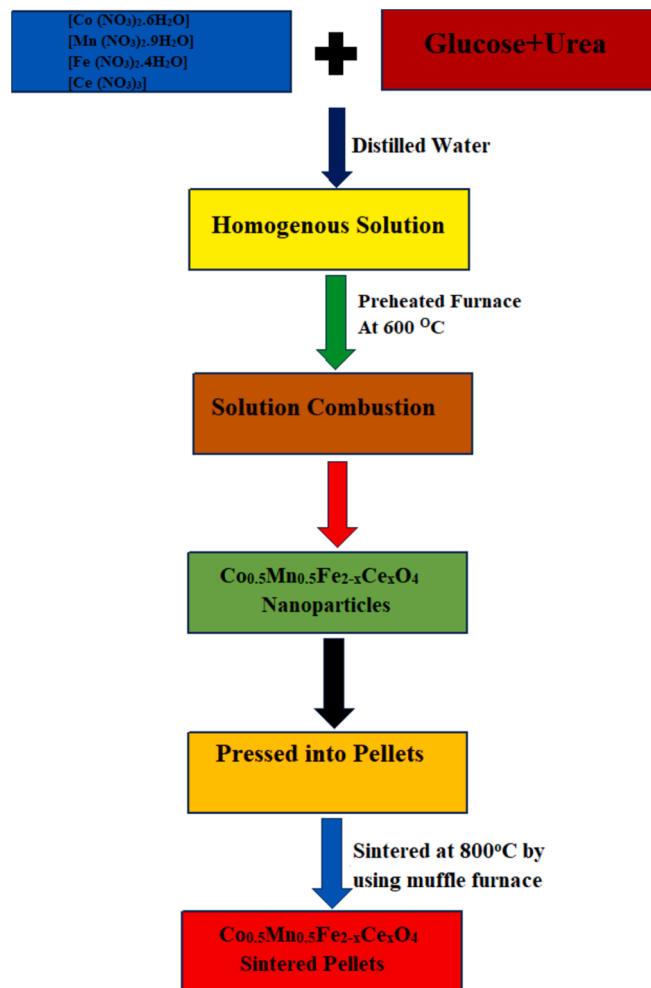


Fig. 1. Flowchart representing the synthesis of $Co_{0.5}Mn_{0.5}Fe_{2-x}Ce_xO_4$ ($x = 0.0, 0.050$, and 0.1) ferrite.

(SEM) (Ultra Scan 60: Japan). X-ray diffraction (XR Ultra Dynamics-400, UK) in the region $2\theta = 20^\circ$ to 80° (Cu $K\alpha$, $\lambda = 1.5418 \text{ \AA}$) was used to determine the crystal structure of synthesized samples. Various chemical and functional groups present in the obtained nano ferrites was analysed through Fourier Transform Infrared Spectroscopy (FTIR) (Thermo Nicolet, Avatar 370 – India). The optical properties in terms of optical absorption for the synthesized ferrites was investigated using UV–visible spectrometry (Perkin Elmer-Canada) in the wavelength range of 200 nm to 800 nm. The experimental setup used to measure the humidity sensing measurement is illustrated in the Fig. 5(a). Pellet samples of 8 mm \times 1.5 mm dimension were prepared applying 5 tons of hydraulic pressure to achieve uniform surface over the pellets surface. The synthesized pellets were sintered at 600 $^\circ\text{C}$ for the duration of 5 h. To establish good level of electrical contact, the silver paste is coated onto sintered pellets. After the post coated pellets were kept in between the two probes humidity sensing chamber using rubber cork and opposite side of the electrode was linked to the programmable computer with advanced digital multimeter (Model: HIOKI) to record the change in sensors resistance as a function of applied humidity.

3. Results and discussion

3.1. SEM analysis

The exterior surface morphologies of the prepared $\text{Co}_{0.5}\text{Mn}_{0.5}\text{Fe}_{2-x}\text{Ce}_x\text{O}_4$ ($x = 0.0, 0.05$ and 0.1) ferrite NPs were investigated by SEM and depicted in Fig. 2(a–c). The SEM micrographs indicate a porous structure with flaky morphologies for the ferrites (Pratibha et al., 2020a,b). The large pores observed in the structure results due to the elimination

of gases during the process of combustion. A smooth and homogeneous morphology was observed for the undoped ferrite sample ($x = 0.0$). The morphological features are affected by the concentrations of Ce^{3+} in the cobalt-manganese-iron oxide ferrites. Among all the samples prepared, $\text{Co}_{0.5}\text{Mn}_{0.5}\text{Fe}_{2-x}\text{Ce}_x\text{O}_4$ ($x = 0.1$) shows highly porous morphology, such kind of porous morphology acts as active sites with improved active surface area and facilitates adsorption of water vapours at active sites. The major enhancement in the pore dimension and pore volume due to the doping of cerium (Ce^{3+}) NPs in $\text{Co}_{0.5}\text{Mn}_{0.5}\text{Fe}_{2-x}\text{O}_4$ ferrite (which is proof via the BET analysis recorded in Table 1).

3.2. XRD analysis

The powder XRD method was used to investigate the structural features of the prepared $\text{Co}_{0.5}\text{Mn}_{0.5}\text{Fe}_{2-x}\text{Ce}_x\text{O}_4$ ($x = 0.0, 0.05$ and 0.1) samples and the XRD patterns are depicted in Fig. 3. The XRD spectra of the ferrite sample shows prominent peaks corresponds to the crystal planes (1 0 0) (1 1 0) (1 1 1) (2 0 0) (2 1 0) (3 0 0) (3 0 1) (3 1 0) and (3 1 1) and shows mono phase cubic crystal structure (JCPDS: Card number: 21–1085). The creation of Fd3m ionic space lattice was confirmed through the XRD patterns. The ionic radius of Ce^{3+} was found to be (1.05 \AA) which is well associated with the radius of Fe^{3+} (0.64 \AA). The Ce^{3+} doping into the ferrite samples does not affect the crystal structure of the host ferrites. To determine the crystallite size, Scherrer's equation (Sunilkumar et al., 2019a,b) which is in well agreement with the grain size obtained through SEM micrographs.

$$D = \frac{k\lambda}{\beta\cos\theta}$$

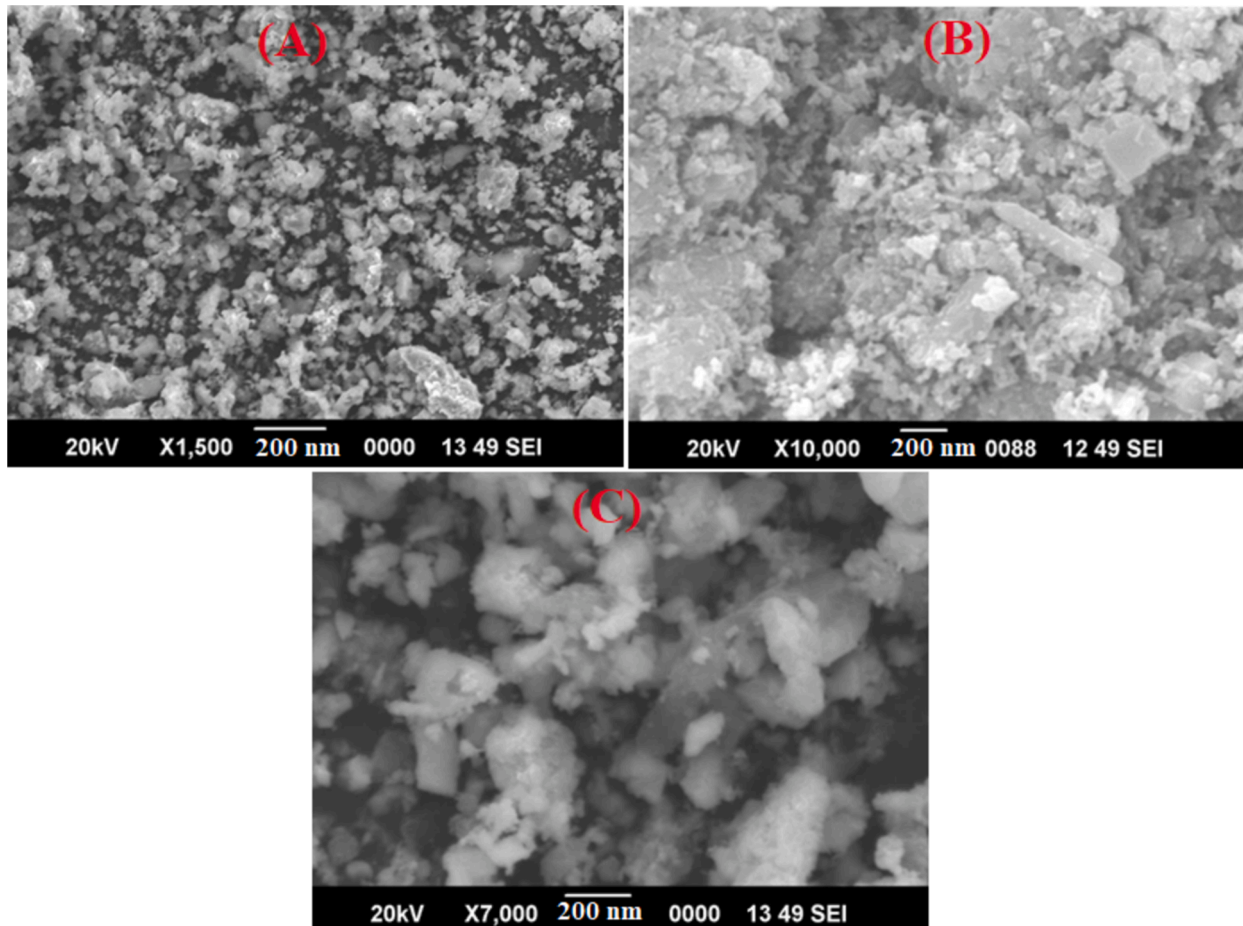
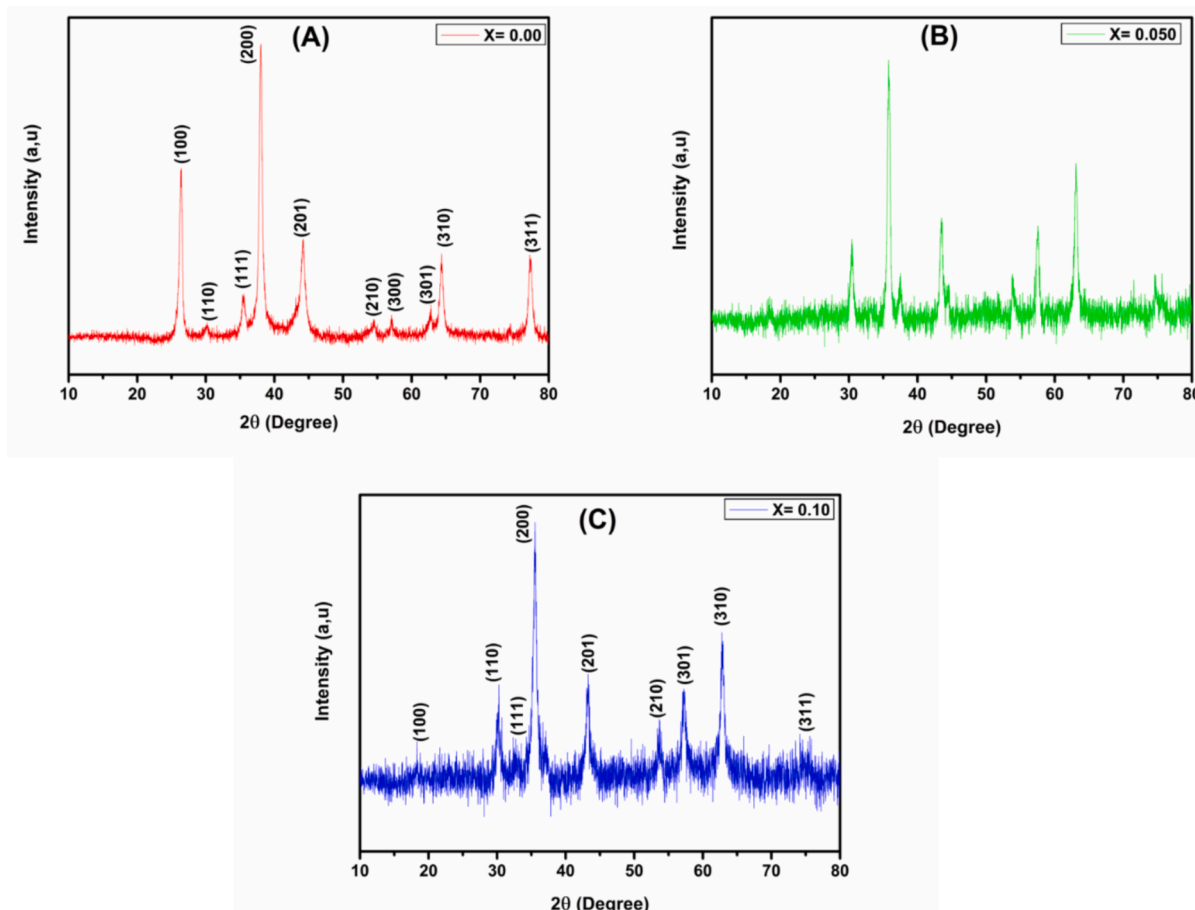


Fig. 2. SEM images of $\text{Co}_{0.5}\text{Mn}_{0.5}\text{Fe}_{2-x}\text{Ce}_x\text{O}_4$ (a) $x = 0.0$ (b) $x = 0.050$ (c) $x = 0.1$ ferrite.

Table 1BET analysis (Surface area, average pore diameter and pore volume) and Humidity sensing parameters for $\text{Co}_{0.5}\text{Mn}_{0.5}\text{Fe}_{2-x}\text{Ce}_x\text{O}_4$ ($x = 0.00, 0.050$ and 0.10) ferrites.

Sl. No	Details of the samples	Surface area (m^2/g)	Average pore diameter (nm)	Pore volume (cm^3/g)	Sensitivity (%)	Response time (Sec)	Recovery time (Sec)	Hysteresis loss (%)
1	X = 0.00	6.2345	1.7853	0.2547	41	94	106	10
2	X = 0.05	17.6543	5.3736	0.4635	62	63	95	7
3	X = 0.10	39.7651	9.4343	0.8239	98	36	63	2

**Fig. 3.** Powder XRD patterns of $\text{Co}_{0.5}\text{Mn}_{0.5}\text{Fe}_{2-x}\text{Ce}_x\text{O}_4$ ($x = 0.0, x = 0.050$ and $x = 0.1$) ferrite.

Here, D represents the crystallite size, k is the parameter depends on the geometry of the sample and is approximately 0.9 for circular particles, where λ is the X-Rays wavelength used, where β is the intensity of FWHM, and θ is the angle of diffraction. The XRD-analysis reveals that, the crystallite size is approximately 40 nm. It was noticed that, lattice parameter and lattice volume parameters show small changes with increasing concentration of Ce^{3+} doping. The spectra obtained by XRD indicates a marginal change in the lattice parameter of $\text{Co}_{0.5}\text{Mn}_{0.5}\text{Fe}_{2-x}\text{Ce}_x\text{O}_4$ ferrite, which results due to the cationic modification in the crystal structure.

It is noticed that, the mean crystallite dimensions were reduced

considerable with increased concentrations of Ce^{3+} owing to lattice distortion in their normal sites. The total volume of the synthesized ferrites samples was determined by employing the equation $V = a^3$ and all determined values are recorded in the Table 2. The strain developed in the synthesized ferrites samples are calculated by using the equation $\epsilon = \frac{\beta \cos \theta}{4}$. The hopping length pertain to magnetic properties such as L_a and L_b are calculated by using the equations $L_A = \frac{a\sqrt{3}}{4}$ and $L_B = \frac{a\sqrt{2}}{4}$ respectively. The hopping lengths are more useful parameters in the estimation of A-site and B-site magnetic ions.

Table 2Structural parameters of $\text{Co}_{0.5}\text{Mn}_{0.5}\text{Fe}_{2-x}\text{Ce}_x\text{O}_4$ (where, $x = 0.00, 0.050$ and 0.1) nano ferrites.

Sl.No	Ce^{3+} Content	Lattice parameter (\AA)	Crystallite size D (nm)	Volume (\AA^3)	Strain ϵ (radian)	Space group	Hopping length	
							L_A	L_B
1	X = 0.00	7.126	32	439.16	2.11×10^{-3}	Fd3m	2.415	1.951
2	X = 0.05	7.176	21	449.26	4.39×10^{-3}	Fd3m	2.482	1.932
3	X = 0.10	7.169	16	445.12	9.42×10^{-3}	Fd3m	2.499	1.931

3.3. FTIR analysis

The FTIR spectra of $\text{Co}_{0.5}\text{Mn}_{0.5}\text{Fe}_{2-x}\text{Ce}_x\text{O}_4$ ($x = 0.0, 0.05$ and 0.1) ferrite is shown in the Fig. 4(d). The characteristic peaks corresponding to 716 cm^{-1} and 528 cm^{-1} stretching frequencies is attributed to the presence of Fe-Mn-O and Co-O bonds related to tetrahedral and octahedral structures of the ferrite. Peaks correspond stretching frequencies of 446 cm^{-1} and 870 cm^{-1} are attributed to the symmetrical lattice vibrations of the cerium, manganese, and cobalt NPs due to their localized sites (Sunilkumar et al., 2019a,b). The characteristic peak near to the stretching frequencies of 2958 cm^{-1} is attributed to the O-H lattice vibration that arise because of absorbed water vapours in the ferrite. Further, the characteristic peaks correspond to frequencies $1644, 1525$ and 1357 cm^{-1} arise due to the vibrations of cobalt-manganese-iron oxide ferrites (Li et al., 2016). Hence, the FT-IR studies confirm the formation of cerium (Ce^{3+}) doped $\text{Co}_{0.5}\text{Mn}_{0.5}\text{Fe}_{2-x}\text{Ce}_x\text{O}_4$ ferrite.

3.4. UV-visible spectroscopic analysis

The UV-visible spectra of $\text{Co}_{0.5}\text{Mn}_{0.5}\text{Fe}_{2-x}\text{Ce}_x\text{O}_4$ ($x = 0.0, 0.05$ and 0.1) NPs investigated in the wavelength regime 200 nm to 800 nm is depicted in the Fig. 4(a-c). By increasing the concentration of cerium (Ce^{3+}) NPs in $\text{Co}_{0.5}\text{Mn}_{0.5}\text{Fe}_{2-x}\text{Ce}_x\text{O}_4$ ferrite, the peak intensity slightly increases. The major absorption peak around 625 nm indicates that, the photons are more absorbed around this wavelength which falls under red region of visible spectrum. In the UV-visible spectra, the energy transition can be due to the $\pi\text{-}\pi^*$ transitions of the ferrite sample (Manjunatha et al., 2019a,b). The band arising from 700 nm in the UV-Vis spectra can be assigned to the free carrier tail.

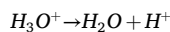
3.5. Humidity sensing studies

Humidity sensing mechanism

The humidity sensing measurements were performed in a laboratory made experimental setup as shown in Fig. 5(a). The humidity sensing mechanism is explained on the base of three possible mechanisms, physisorption, chemisorption and followed by capillary condensation. Initially, the water vapour gets ionized in the form of H^+ and OH^- ions and get adsorbed over the surface of sensing material (Ravikiran et al., 2018).



During first stage of physisorption, the well distinguished OH^- ions gets linked to the sensing surface and chemisorption layer and H^+ ions are liberated from the sensing material. The OH^- ions which are chemisorbed form a strong hydrogen bond with the nearby water molecule to result (H_3O^+). The released H^+ ion start to migrate between water molecules forming the hydrogen bonds. This entire mechanism take place as per the Grotthuss chemical mechanism (Zhang et al., 2018).



By enhancing the RH%, the physisorbed water vapour gets collected on the sensing surface creating the second step of physisorption mechanism. At the end step the adsorbed water vapours get collected in the capillary tubes which enhanced the protonation mechanism in the ferrite which results in the improved humidity sensing performance of

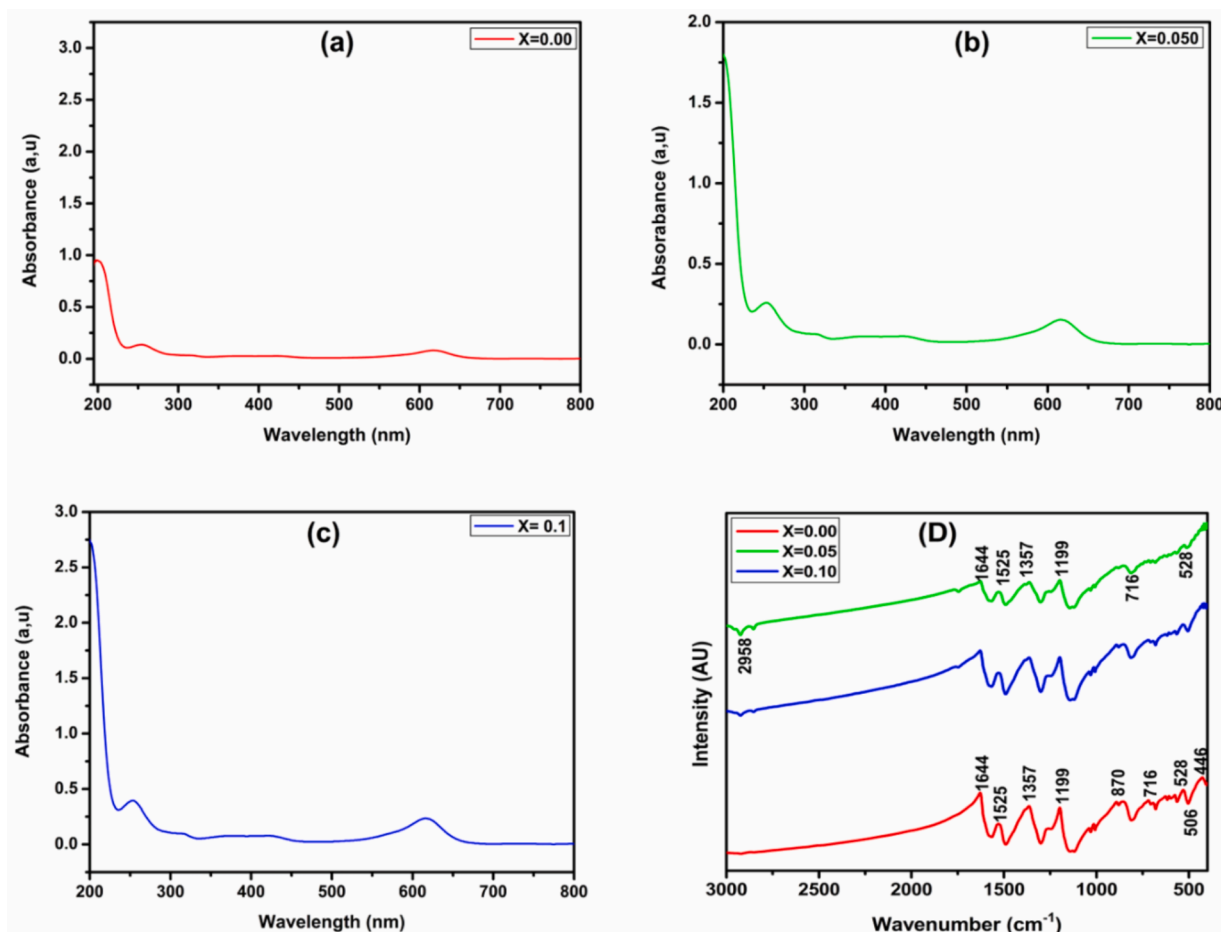


Fig. 4. (a-c) UV-Vis spectra and (d) FT-IR spectra for $\text{Co}_{0.5}\text{Mn}_{0.5}\text{Fe}_{2-x}\text{Ce}_x\text{O}_4$ ($x = 0.0, x = 0.050$ and $x = 0.1$) ferrite.

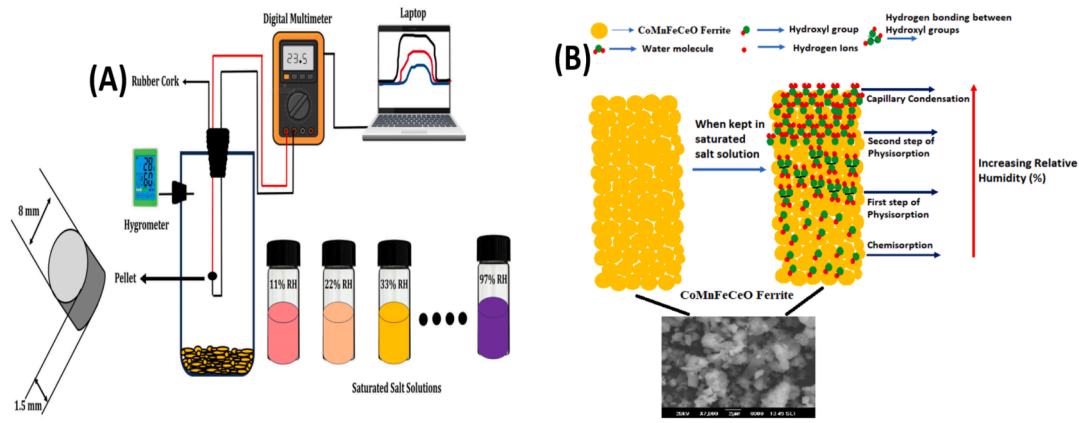


Fig. 5. (A) Humidity sensing set-up used in the present investigation (B) Humidity sensing mechanism at the ferrite surface.

the ferrites. Over all these outcomes which results into reduction of the resistance values and thus enhances in its humidity sensing performance of the ferrite (Sarwar Hasan et al., 2022). The detailed humidity sensing mechanism of prepared ferrites sample was illustrated in the Fig. 5(b).

3.6. Variation of resistance with relative humidity

The change of sensors resistance with a function of relative humidity (%) for $\text{Co}_{0.5}\text{Mn}_{0.5}\text{Fe}_{2-x}\text{Ce}_x\text{O}_4$ ($x = 0.0, 0.05$ and 0.1) ferrite were illustrated in the Fig. 6(a). One can easily observe from the plots that the sensors resistance drops considerably with increasing relative humidity (RH) from 12 % RH to 97 % RH due to the more adsorption of water vapours over the surface of ferrite. This could be due to two prime reasons, first, the adsorbed moisture being comparatively lower because of which water molecules do not follow the change in electric filed direction and second, resistance lean on the geometry of the sample (Shah et al., 2011).

Among the synthesized ferrite the highest change in sensors resistance was observed at 12 % RH for $\text{Co}_{0.5}\text{Mn}_{0.5}\text{Fe}_{2-x}\text{Ce}_x\text{O}_4$ ($x = 0.1$) NPs concentration. The humidity sensitivity for different humidity at

ambient temperature for the $\text{Co}_{0.5}\text{Mn}_{0.5}\text{Fe}_{2-x}\text{Ce}_x\text{O}_4$ ($x = 0.0, 0.05$ and 0.1) ferrite determined by employing the below formula (Kotnala et al., 2008).

$$\text{Humidity sensing response (\%)} = \left[\frac{R_{LH} - R_H}{R_{LH}} \right]$$

where the resistance at lower humidity level represented by R_{LH} and the resistance due to variable relative humidity is R_H .

3.7. Variation of capacitance with relative humidity

The trend of capacitance with applied relative humidity for $\text{Co}_{0.5}\text{Mn}_{0.5}\text{Fe}_{2-x}\text{Ce}_x\text{O}_4$ ($x = 0.00, 0.5$ and 0.1) ferrite recorded at a constant frequency of 100 Hz at ambient temperature is shown in Fig. 6 (b). From the plots we can simply observed that the capacitance of the ferrite improved with increasing % of RH. In the beginning, up to 30 % RH the capacitance value remains the same, later at higher frequency region the capacitance value exponentially increases with higher RH was noticed due to more adsorption of water molecules which facilitates

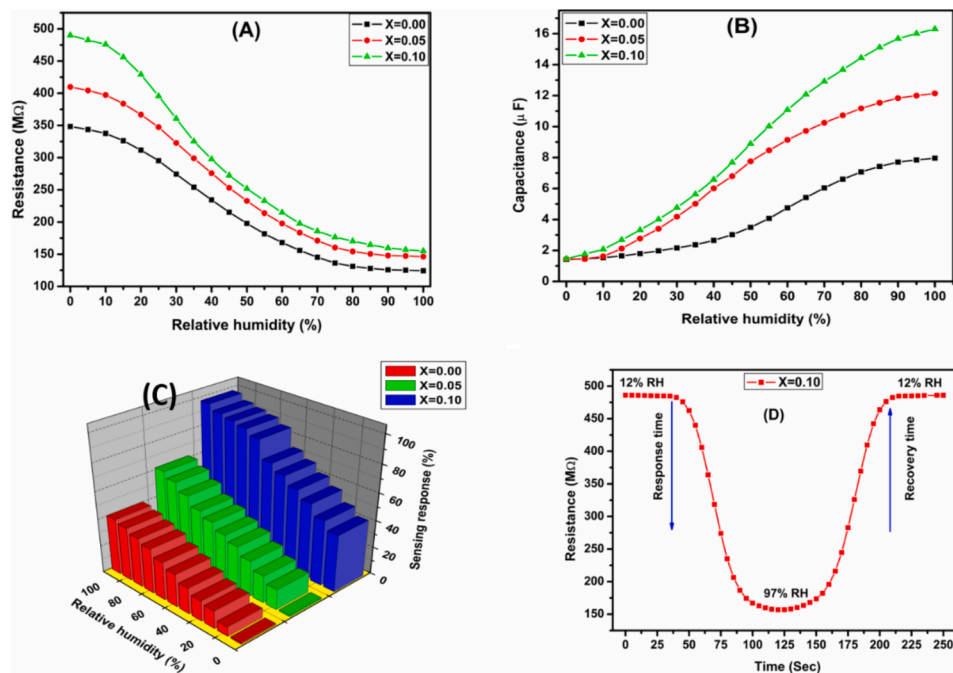


Fig. 6. (A) Change in resistance (B) Change in Capacitance (C) Sensing response as a function of Relative humidity for $\text{Co}_{0.5}\text{Mn}_{0.5}\text{Fe}_{2-x}\text{Ce}_x\text{O}_4$ ($x = 0.0, x = 0.050$ and $x = 0.1$) ferrite (D) Dynamic sensing response.

the accumulation of charge carriers inside the host ferrite. According to the adsorption theory, the adsorption of water molecules occur in two variable methods. The first step related to chemisorption mechanism and second step is physisorption mechanism. The additional layer on the sensing ferrite sample influences the capacitance change in the ferrite. It was found experimentally that the capacitance of the ferrite is directly proportional to the conductance and inversely proportional to the electric field (Syed Khasim et al., 2021). Among all the synthesized ferrites $\text{Co}_{0.5}\text{Mn}_{0.5}\text{Fe}_{2-x}\text{Ce}_x\text{O}_4$ ($x = 0.1$) sample exhibited higher capacitance and which results into more humidity sensitivity.

3.8. Humidity sensing performance with relative humidity

The trend of humidity sensing response as a function of relative humidity (%) recorded at ambient temperature for $\text{Co}_{0.5}\text{Mn}_{0.5}\text{Fe}_{2-x}\text{Ce}_x\text{O}_4$ ($x = 0.0, 0.05$ and 0.1) ferrite were illustrated in the Fig. 6(c). It is clearly observed from the plots that the humidity sensing response enhances with relative humidity from 12 % to 97 % (Srinivasamurthy et al., 2023). The humidity sensing response in the present work is better than that of nickel-iron-zinc oxide ferrite NPs synthesized via solution combustion technique (Apsar Pasha and Angadi, 2023). Among the prepared ferrite $\text{Co}_{0.5}\text{Mn}_{0.5}\text{Fe}_{2-x}\text{Ce}_x\text{O}_4$ ($x = 0.1$) sample shows maximum humidity sensing responses of 98 % in comparison to other synthesized ferrite samples. The doping of cerium (Ce^{3+}) NPs into the cobalt-manganese-iron oxide ferrite leads to the enhanced porosity and larger absorption of water molecules and hence improved sensing response.

3.9. Humidity response and recovery times

The humidity sensing response and recovery times were defined as, the time taken to achieve 90 % of humidity sensitivity (saturation) at the time one complete gasification process and the same time the degasification mechanism was utilized to measure the sensor recovery times when the humidity sensitivity drop to baseline. The response and recovery plots for $\text{Co}_{0.5}\text{Mn}_{0.5}\text{Fe}_{2-x}\text{Ce}_x\text{O}_4$ ($x = 0.1$) ferrites studied at room temperature is shown in the Fig. 6(d). To measure the response and recovery times two sensing chambers were used, the first chamber which comprises of 11 % RH and other chamber comprises of 95 % RH. The sensing response for $\text{Co}_{0.5}\text{Mn}_{0.5}\text{Fe}_{2-x}\text{Ce}_x\text{O}_4$ ($x = 0.1$) sample was found to be 36 s when the sample was shifted from 12 % RH to 97 % RH and at the same time the recovery time 63 s was measured when the tested sample moved from 97 % RH to 12 % RH. The improved response and recovery times of $\text{Co}_{0.5}\text{Mn}_{0.5}\text{Fe}_{2-x}\text{Ce}_x\text{O}_4$ ferrite material can be used as an efficient material in the design of humidity sensors (Hiremath et al., 2023). The main reason for the improved response and recovery time in $\text{Co}_{0.5}\text{Mn}_{0.5}\text{Fe}_{2-x}\text{Ce}_x\text{O}_4$ ferrite was believed that doping of rare earth nanoparticles like cerium into the $\text{Co}_{0.5}\text{Mn}_{0.5}\text{Fe}_{2-x}\text{Ce}_x\text{O}_4$ ferrite which turn to more porous morphology which facilitate more absorption of water molecules over the surface of ferrite sample and it causes improved response and recovery times (Syed Khasim et al., 2023). The

Comparative analysis of Humidity sensing performance of different ferrites-based composites synthesized via different methods with the recently published works were given in the Table 3.

3.10. Humidity hysteresis

The humidity hysteresis curves for $\text{Co}_{0.5}\text{Mn}_{0.5}\text{Fe}_{2-x}\text{Ce}_x\text{O}_4$ ($x = 0.0, 0.05, 0.1$) ferrite were recorded in the regime of 11 % RH to 98 % RH as illustrated in the Fig. 7(a-c). The adsorption trend exhibited by slowly enhancing from the relative humidity range 11 % to 98 % and desorption curve is back tracing at the time of measurement. It was very curious to observe from the hysteresis plots, the desorption mechanism little slower in compare to the adsorption mechanism. This recommends that the exothermic and endothermic responses of the sensors are well compared to the adsorption and desorption mechanism occurs at different rates leading to the lower the impedance value in desorption mechanism in compare to the adsorption mechanism. Among the prepared ferrite $\text{Co}_{0.5}\text{Mn}_{0.5}\text{Fe}_{2-x}\text{Ce}_x\text{O}_4$ ($x = 0.1$) sample shows lower hysteresis loss in the order of 2 % in compare to the other synthesized ferrites samples, this kind of behaviour might be due the improved morphological features and higher humidity sensitivity (Ramakrishna et al., 2023). The humidity hysteresis loss of the synthesized ferrites can be calculated by using the equation.

$$\text{Hysteresis}(\%) = \left[\frac{a - b}{Y_{\max} - Y_{\min}} \right]$$

In the above equation, "a" be the highest value and "b" be the lowest value of Y at the overage of the % relative humidity. All the humidity sensing parameters of the synthesized materials are shown in Table 1.

3.11. Stability analysis

In this test, we have tested $\text{Co}_{0.5}\text{Mn}_{0.5}\text{Fe}_{2-x}\text{Ce}_x\text{O}_4$ ($x = 0.1$) ferrite at relative humidity of 30 % and 97 % for each 8 days in 90 days' time interval. Fig. 7(d) shows the stability plots of 30 % and 97 % RH for $\text{Co}_{0.5}\text{Mn}_{0.5}\text{Fe}_{2-x}\text{Ce}_x\text{O}_4$ ($x = 0.1$) ferrite recorded at ambient temperature. From the plots clearly shows that, in both humidity condition the synthesized ferrite sample exhibited outstanding stable performance over a long period with negligible loss of sensitivity which is nearly 2 %, this least loss in humidity sensitivity might be due to the aging induced effect was observed in most of the ferrites-based sensors. Therefore, the stability test indicated that, the prepared humidity sensing material is showing the outstanding stable performance at higher concentration of cerium doped cobalt-manganese-iron ferrite at ambient temperature (Syed Khasim et al., 2024). The lower concentration cerium NPs doped cobalt-manganese-iron ferrite was not examined the stability analysis, because these composites show lower humidity sensitivity in compared to the $\text{Co}_{0.5}\text{Mn}_{0.5}\text{Fe}_{2-x}\text{Ce}_x\text{O}_4$ ($x = 0.1$) ferrite. However, the lower humidity sensing ferrite materials could find potential applications especially in energy storage, optoelectronic and electronic applications (Ramakrishna et al., 2024).

Table 3

Comparative analysis of Humidity sensing performance of different ferrites-based composites in recently published works.

Sl. No	Details of ferrites sample	Synthesis method	Measurement range (RH)	Sensing response	Response and recovery times (s)	Reference
1	Scandium doped cobalt chromate	Solution combustion	40 %–90 %	67 %	66/103	(Manjunatha et al., 2019a, b)
2	Cobalt-Nickel-Iron doped Caesium ferrites	Solvothermal	10 %–80 %	76 %	78/120	(Srinivasamurthy et al., 2023)
3	Rubidium-doped Magnesium ferrite	Chemical combustion	30 %–90 %	61 %	95/130	(Hiremath et al., 2022)
4	Praseodymium doped magnesium ferrite	Electrochemistry method	5 %–60 %	86 %	45/68	(Shah et al., 2011)
5	Samarium doped Lanthanum Aluminate	Hydrothermal method	15 %–80 %	88 %	48/78	(Pratibha et al., 2020a,b)
6	$\text{Co}_{0.5}\text{Mn}_{0.5}\text{Fe}_{2-x}\text{Ce}_x\text{O}_4$	Solution combustion	11 %–98 %	98 %	36/63	Present work

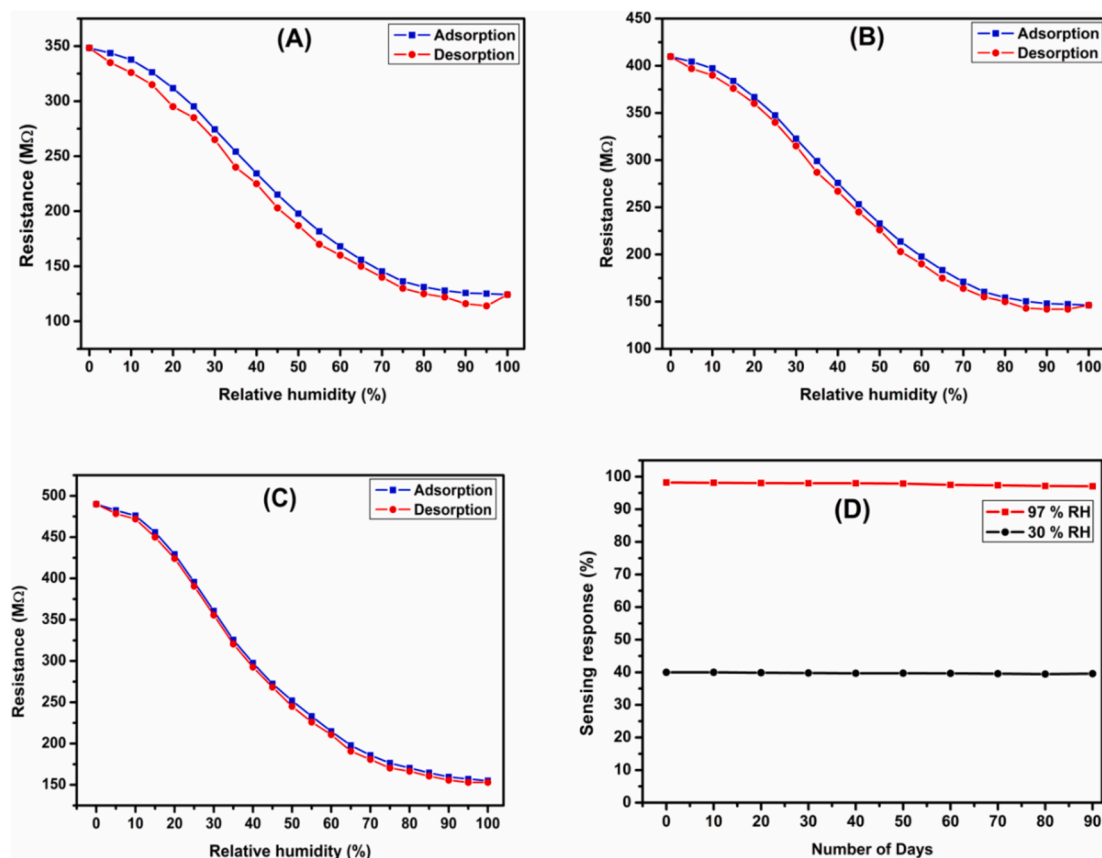


Fig. 7. (A–C) Humidity hysteresis characteristics $\text{Co}_{0.5}\text{Mn}_{0.5}\text{Fe}_{2-x}\text{Ce}_x\text{O}_4$ ($x = 0.0$, $x = 0.050$ and $x = 0.1$) ferrite (D) Stability study for $x = 0.1$ ferrite.

4. Conclusion

In conclusion, cerium (Ce^{3+}) doped cobalt-manganese-iron oxide ferrites were synthesized using simple solution combustion technique. The Ce^{3+} and Fe^{3+} NPs were successfully doped with different concentrations into the host cobalt-manganese oxide ferrite system, without changing the phase of host ferrites. The XRD studies confirms the presence of major crystal planes and formation of cubic spinel structure in doped ferrites. The SEM studies suggest a porous flaky surface morphology for the doped ferrites. The presence of both the elements dopant and host ferrite was confirmed through FT-IR and UV-Vis studies. By doping the cerium (Ce^{3+}) into host ferrites facilitates the formation of porous structure which serves as vapour absorption sites. The Ce^{3+} doping in the host ferrites increases the humidity sensing response of the ferrite samples. Among the series of ferrite samples synthesized, $\text{Co}_{0.5}\text{Mn}_{0.5}\text{Fe}_{2-x}\text{Ce}_x\text{O}_4$ ($x = 0.1$) ferrite shows improved sensitivity with quick response and recovery times. Further, the Ce^{3+} doped ($x = 0.1$) sample exhibits long term stability (90 days) without deteriorating its sensing response. Hence, the $\text{Co}_{0.5}\text{Mn}_{0.5}\text{Fe}_{2-x}\text{Ce}_x\text{O}_4$ ($x = 0.1$) ferrite synthesized in the present investigation could potentially be used to fabricate a resistive type humidity sensor. Owing to its easy synthesis, superior sensing response, short response/recovery time as well as long-term stability, the humidity sensors fabricated in this study using $\text{Co}_{0.5}\text{Mn}_{0.5}\text{Fe}_{2-x}\text{Ce}_x\text{O}_4$ ($x = 0.1$) ferrite could open new avenues for sensor technology.

CRedit authorship contribution statement

S.A. Al-Ghamdi: Writing – review & editing, Writing – original draft, Methodology, Investigation, Formal analysis, Data curation, Conceptualization.

Declaration of competing interest

The authors declare that they have no known competing financial interests or personal relationships that could have appeared to influence the work reported in this paper.

References

- Ahиландeswari, Sakthipandi, E., Kanna, R.R., Rajkumar, G., Babu, B.G., Arunmetha, S., Hossain, A., Sakthivel, P., Rajendran, V., Srinidhi Raghavan, M., 2023. Exploring the electromagnetic shielding behavior of lanthanum doped calcium nanoferrites. *J. Rare Earths*. <https://doi.org/10.1016/j.jre.2023.11.002>.
- Ali, R., Mahmood, M.A., Khan, A.H., Chughtai, M., Shahid, I., Shakir, M.F.W., 2014. Impacts of Ni-Co substitution on the structural, magnetic, and dielectric properties of magnesium nano-ferrites fabricated by micro-emulsion method. *J. Alloy. Compd.* 584, 363–368.
- Angadi, V.J., Manjunatha, K., Praveena, K., Pattar, V.K., Fernandes, B.J., Manjunatha, S. O., Husain, J., Angadi, S.V., Horakeri, L.D., Ramesh, K.P., 2021. Magnetic properties of larger ionic radii samarium and gadolinium doped manganese zinc ferrite nanoparticles prepared by solution combustion method. *J. Magn. Magn. Mater.* 529, 167899.
- Apsar Pasha, V., Angadi, J., 2023. Role of post-transition metal (Bi2O3) on the structural, microstructural, and Humidity Sensing Behaviour of Bi@Zinc ferrites composite for room temperature operatable humidity sensors. *J. Electron. Mater.* Mater. Electron. 34. <https://doi.org/10.1007/s10854-023-10392-z>.
- Blank, T., Eksperianova, L.P., Belikova, K.N., 2016. Recent trends of ceramic humidity sensors development: a review. *Sens. Actuators B Chem.* 228, 416–442.
- Chethan, B., Prakash, H.G.R., Ravikiran, Y.T., Vijayakumari, S.C., Thomas, S., 2019. Polypyrrole based core-shell structured composite-based humidity sensor operable at room temperature. *Sens. Actuators B Chem.* 296, 126639.
- Hasan, S., et al., 2022. Thermo-dielectric humidity, dielectric and humidity sensing properties of barium mono-ferrite and barium hexaferrites nanoparticles. *Results Phys.* 42, 105962.
- Hiremath, V.G., et al., 2023. Enhanced humidity sensing stability of Dy^{3+} -doped Mg-Rb ferrites for room temperature operatable humidity sensor applications. *J. Mater. Sci. Mater. Electron.* 34, 1537. <https://doi.org/10.1007/s10854-023-10936-3>.
- Hiremath, V.G., Yahia, I.S., Zahran, H.Y., 2022. Humidity sensing behaviour of Rubidium-doped Magnesium ferrite for sensor applications. *J. Mater. Sci. Mater. Electron.* 33, 11591–11600. <https://doi.org/10.1007/s10854-022-08131-x>.

- Jagadeesha Angadi, V.A.V., Anupama, R., Kumar, S., Matteppanavar, B., Rudraswamy, B. S., 2016. Observation of enhanced magnetic pinning in Sm^{3+} substituted nanocrystalline Mn-Zn ferrites prepared by propellant chemistry route. *J. Alloy. Compd.* 682, 263–274.
- Jagadeesha Angadi, V., Lakshmi, H.R., Manjunatha, K., 2020. Investigation of Structural, Microstructural, Dielectrical and Magnetic Properties of Bi^{3+} Doped Manganese Spinel Ferrite Nanoparticles for Photonic Applications Bismuth – Fundamentals and Photonic Applications (IntechOpen, London, 2020).
- Kanna, R., Sakthipandi, K., Lenin, N.E., Jebaseelan Samuel, James, 2019. Neodymium doped on the manganese-copper nanoferrites: analysis of structural, optical, dielectric, and magnetic properties. *J. Mater. Sci. Mater. Electron.* 30, 4473–4486.
- Khasim, S., Pasha, A., Badi, N., Lakshmi, M., Al-Aoh, H., 2021. PVA treated PEDOT:PSS: TiO_2 nanocomposite based high-performance sensors towards detection of relative humidity and soil moisture content for agricultural applications. *J. Polym. Environ.* 29, 612–623. <https://doi.org/10.1007/s10924-020-01905-6>.
- Khasim, S., Pasha, A., Dastager, S.G., Panneerselvam, C., Hamdallah, T.A., Al-Ghamdi, S. A., Alfadli, S.A., Makandar, M.B., Darwish, A.A.A., 2023. Design and development of multi-functional graphitic carbon nitride heterostructures embedded with copper and iron oxide nanoparticles as versatile sensing platforms for environmental and agricultural applications. *Ceram. Int.* 49, 20688–20698.
- Kotnala, R.K., Shah, J., Singh, B., Singh, S., Dhawan, S.K., Sengupta, A., 2008. Humidity response of Li-substituted magnesium ferrite. *Sens. Actuators B Chem.* 129, 909–914. <https://doi.org/10.1016/j.snb.2007.10.002>.
- Lakshmi, H.R., Manjunatha, K., Husain, J., 2020. Effect of cerium on structural, microstructural, magnetic and humidity sensing properties of Mn–Bi ferrites. *Nano-Struct. Nano-Objects* 24, 100608.
- Li, Y., Fan, K., Ban, H., Yang, M., 2016. Detection of very low humidity using polyelectrolyte/graphene bilayer humidity sensors. *Sens. Actuators B Chem.* 222, 151–158.
- Lodhi, M.Y., Mahmood, K., Mahmood, A., Malik, H., Warsi, M.F., Shakir, I., Asghar, M., Khan, M.A., 2014. New $\text{Mg}_{0.5}\text{Co}_x\text{Zn}_{0.5-x}\text{Fe}_2\text{O}_4$ nano-ferrites: structural elucidation and electromagnetic behaviour evaluation. *Curr. Appl. Phys.* 14, 716–720.
- Manikandan, V., Samiksha Sikarwar, B.C., Yadav, R.S.M., 2018. Fabrication of tin substituted nickel ferrite ($\text{Sn-NiFe}_2\text{O}_4$) thin film and its application as opto-electronic humidity sensor. *Sens. Actuators A* 272, 267–273. <https://doi.org/10.1016/j.sna.2018.01.059>.
- Manjunatha, K., et al., 2019a. Observation of enhanced humidity sensing performance and structure, dielectric, optical and DC conductivity studies of scandium doped cobalt chromate. *J. Mater. Sci.: Mater. Electron.* 30, 17202–17217.
- Manjunatha, K., et al., 2020. Exploring the structural, dielectric, and magnetic properties of 5 Mol% Bi^{3+} -substituted CoCr_2O_4 nanoparticles. *J. Supercond. Nov. Magn.* 71, 1–12.
- Manjunatha, K., Ho, M.K., Hsu, 2024. Structure, microstructure, and enhanced sensing behavior of nickel ferrite–cobalt chromate for humidity sensor applications. *J. Mater. Sci. Mater. Electron.* 35, 471. <https://doi.org/10.1007/s10854-024-12198-z>.
- Manjunatha, S., Machappa, T., Ravikiran, Y.T., Chethan, B., Sunilkumar, A., 2019b. Polyaniline based stable humidity sensor operable at room temperature. *Phys. B Condens. Matter* 561, 170.
- Pratibha, S., Dhananjayaa, N., Pasha, A., Khasim, S., 2020a. Improved luminescence and LPG sensing properties of Sm^{3+} doped Lanthanum aluminate thin films. *Appl. Nanosci.* 10, 1927–1939.
- Pratibha, S., Chethan, B., Ravikiran, Y.T., Dhananjaya, N., Jagadeesh Angadi, V., 2020b. Enhanced humidity sensing performance of Samarium doped Lanthanum Aluminate at room temperature. *Sens. Actuators A Phys.* 304, 111903.
- Ramakrishna, B.N., Pasha, A., Khasim, S., Manjunatha, S.O., 2023. LPG sensing behaviour and dielectric properties of lanthanum doped cobalt-iron oxide ferrite nano composites sensors operated at room temperature at ppb level. *Ceram. Int.* 49 (24, Part A 15), 40775–40786.
- Ramakrishna, B.N., Pasha, A., Khasim, S., 2024. Improved broad band electromagnetic interference shielding and strain sensing properties of multifunctional reduced Graphene Oxide/Iron-Cobalt ferrite composites. *J. Electron. Mater.* 53, 48. <https://doi.org/10.1007/s10854-023-11781-0>.
- Ravikiran, Y.T., Raj, B.C.H.G., Vijaya, P.S.C., Thomas, K.S., 2018. Effect of mechanical mixing method of preparation of polyaniline- transition metal oxide composites on DC conductivity and humidity sensing response. *J. Mater. Sci. Mater. Electron.* 29, 2–10.
- Rezlescu, N., Rezlescu, E., Popa, P.D., Tudorache, F., 2005. A model of humidity sensor with a mg-based ferrites. *J. Optoelectron. Adv. Mater.* 7, 907–910.
- Sakthipandi, K., Babu, B.G., Rajkumar, G., Hossian, A., Raghavan, M.S., Kumar, M.R., 2022. Investigation of magnetic phase transitions in $\text{Ni}_0.5\text{Cu}_0.25\text{Zn}_0.25\text{Fe}_2\text{-xLaxO}_4$ nanoferrites using magnetic and in-situ ultrasonic measurements. *Phys. B Condens. Matter* 645, 414280.
- Sathisha, C., Manjunatha, K., Angadi, V.J., Reddy, R.K., 2020. Structural, microstructural, electrical, and magnetic properties of $\text{CuFe}_{2-(x+y)}\text{Eu}_x\text{Sc}_y\text{O}_4$ (where x and y vary from 0 to 0.03) Nanoparticles. *J. Supercond. Nov. Magn.* 33, 3963–3973.
- Shah, J., Arora, M., Purohit, L.P., Kotnala, R.K., 2011. Significant increase in humidity sensing characteristics of praseodymium doped magnesium ferrite. *Sens. Actuators A Phys.* 167, 332–337. <https://doi.org/10.1016/j.sna.2011.03.010>.
- Srinivasamurthy, K.M., Pasha, Apsar, Jagadeesha Angadi, V., Manjunatha, K., 2023. LPG sensing and Humidity sensing studies of gamma irradiated $\text{Co}_0.5\text{Ni}_0.5\text{Ce}_0.01\text{Fe}_1.99\text{O}_4$ nanocomposite thin film for sensor application. *J. Electron. Mater.* 52, 471. <https://doi.org/10.1007/s10854-022-09658-9>.
- Sunilkumar, A., Manjunatha, S., Machappa, T., Chethan, B., Ravikiran, Y.T., 2019a. A tungsten disulphide–polypyrrole composite-based humidity sensor at room temperature. *Bull. Mater. Sci.* 42, 1–5.
- Sunilkumar, A., Manjunatha, S., Chethan, B., Ravikiran, Y.T., Machappa, T., 2019b. Polypyrrole-Tantalum disulfide composite: an efficient material for fabrication of room temperature operable humidity sensor. *Sens. Actuators A Phys.* 298, 111593.
- Syed Khasim, B.N., Ramakrishna, A.P., Manjunatha, S.O., 2024. Structural, optical, magnetic, and electrical properties of samarium (Sm^{3+}) doped copper-iron oxide ferrites for possible opto-electronic applications. *J. Electron. Mater.* <https://doi.org/10.1007/s11664-023-10797-w>.
- Zhang, D., Wang, D., Li, P., Zhou, X., Zong, X., Dong, G., 2018. Facile fabrication of high-performance QCM humidity sensor based on layer-by-layer self-assembled polyaniline/graphene oxide nanocomposite film. *Sens. Actuators B Chem.* 255, 1869–1877.